

Headline Articles

Dimerization Effect on the Physical Properties in New One-Dimensional Organic Conductors: $(ChTM\text{-}TTP)_2AuBr_2$, $(ChTM\text{-}TTP)_2GaCl_4$, and $(ChTM\text{-}TTP)ReO_4$

Tadashi Kawamoto,* Minoru Ashizawa, Takehiko Mori, Jun-Ichi Yamaura,† Reizo Kato,†† Yohji Misaki,††† and Kazuyoshi Tanaka†††

Department of Organic and Polymeric Materials, Graduate School of Science and Engineering, Tokyo Institute of Technology, O-okayama, Meguro-ku, Tokyo 152-8552

†Institute for Solid State Physics, The University of Tokyo, Kashiwanoha, Kashiwa-shi, Chiba 277-8581

††RIKEN, The Institute of Physical and Chemical Research, Hirosawa, Wako-shi, Saitama 351-0198

†††Department of Molecular Engineering, Graduate School of Engineering, Kyoto University, Yoshida, Kyoto 606-8501

(Received August 20, 2001)

Crystal structure analyses, measurements of transport and magnetic properties, and low-temperature X-ray studies of new organic conductors: $(ChTM\text{-}TTP)_2AuBr_2$, $(ChTM\text{-}TTP)_2GaCl_4$, and $(ChTM\text{-}TTP)ReO_4$, where ChTM-TTP is 2-[4,5-(1,2-cyclohexylenedithio)-1,3-dithiol-2-ylidene]-5-[4,5-bis (methylthio)-1,3-dithiol-2-ylidene]-1,3,4,6-tetrathiapentalene, have been carried out. In these compounds, the donors form quasi-one-dimensional columns with dimerization induced by the steric hindrance of the 1,2-cyclohexylene unit. The crystal structures and the energy band structures of both $AuBr_2^-$ and $GaCl_4^-$ salts are similar to those of the Bechgaard salts. The electrical resistivity and the thermoelectric power show metallic behavior above 100 K for the $AuBr_2^-$ salt and above 150 K for the $GaCl_4^-$ salt. The results of the ESR spin susceptibility, the static magnetic susceptibility, and the low-temperature X-ray studies indicate that the ground states of both salts are antiferromagnetic insulators. The Néel temperatures are about 38 K for the $AuBr_2^-$ salt and about 32 K for the $GaCl_4^-$ salt. These salts are the first materials showing an antiferromagnetic state among the TTP series conductors. In $(ChTM\text{-}TTP)_2X$ (X = $Au(CN)_2$, $AuBr_2$, and $GaCl_4$), the strength of the dimerization is related to the charge localization temperature. For the ReO_4^- salt, the donor to anion ratio is 1:1 in spite of the tetrahedral anion being similar to the $GaCl_4^-$ anion. Although the interstack interactions are not small, the degree of charge transfer of the donor molecule is +1; thus this salt has an energy gap at the Fermi level, in agreement with the semiconducting transport behavior.

In the history of the study of organic conductors, the TMT*C*F salts (C = S: tetramethyltetrathiafulvalene, C = Se: tetramethyltetraselenafulvalene) have attracted a great deal of attention because of their various one-dimensional physical phenomena; below 20 K $(TMTCF)_2X$ (X = PF_6, AsF_6, Br, and ClO_4) undergo transitions to such ground states as the spin-Peierls (nonmagnetic), spin density wave (antiferromagnetic), and superconducting states.[1–3] As for the two-dimensional system, BEDT-TTF (bis(ethylenedithio)tetrathiafulvalene) makes a rich variety of molecular arrangements depending on the anion shape or size.[4,5] In these organic conductors, the dimerization realizes the effectively half-filled band in the 2:1 composition, which is crucial to the appearance of the above important ground states.

Bis-fused TTF donors, called TTP (tetrathiapentalene) series donors, have been synthesized and a large number of radical-cation salts have been obtained. Many radical-cation salts of the TTP series donors show metallic behavior down to liquid He temperatures.[6] In organic conductors based on TTP series donors, only $(DTEDT)_3Au(CN)_2$ (DTEDT: 2-(1,3-dithiol-2-ylidene)-5-[2-(1,3-dithiol-2-ylidene)-ethylidene]-1,3,4,6-tetrathiapentalene) shows superconductivity below 4 K at ambient pressure.[7] The TTP series donors have a strong tendency to

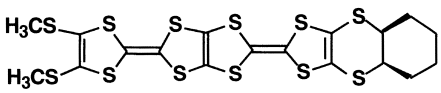

ChTM-TTP

Scheme 1.

construct uniform stacks and quasi-two-dimensional electronic structures. The uniform stacking pattern realized in these conductors does not appear to depend on the anion shape or size, and is unfavorable to the appearance of magnetic or superconducting phase transitions.

In an attempt to introduce dimerization, ChTM-TTP (see Scheme 1) has been synthesized by attaching a bulky substituent, a cyclohexane ring.[8] (ChTM-TTP)$_2$Au(CN)$_2$ has a dimerized structure because of the steric hindrance of the 1,2-cyclohexylenedithio ring with large bending. At the same time, the electronic structure becomes quasi-one-dimensional, in contrast to the two-dimensionality in other TTP salts. This compound shows metallic behavior down to 120 K and successively undergoes a magnetic phase transition around 40 K.[8–10] This suggests that the introduction of a bulky substituent is useful to obtain the dimerized 2:1 salts in the TTP series donors. In order to investigate the effect of anion size and shape as well as the role of the cyclohexane ring attached in cis conformation, we have prepared ChTM-TTP salts with a linear anion ($AuBr_2^-$) and tetrahedral anions ($GaCl_4^-$ and ReO_4^-).

In the present paper, crystal structures, energy band structures, transport properties, magnetic properties, and low-temperature X-ray studies of three new compounds: (ChTM-TTP)$_2$AuBr$_2$, (ChTM-TTP)$_2$GaCl$_4$, and (ChTM-TTP)ReO$_4$ will be shown and discussed in comparison with (ChTM-TTP)$_2$Au(CN)$_2$ and other organic conductors. The $AuBr_2^-$ salt is strictly isostructural to the $Au(CN)_2^-$ salt, and the $GaCl_4^-$ salt has an essentially similar quasi-one-dimensional energy band, though the interchain donor arrangement is modified. (ChTM-TTP)ReO$_4$ has a similar dimerized structure, but is a 1:1 band insulator. This work demonstrates that the strength of the dimerization plays an important role in determining the properties of the ChTM-TTP salts.

Although the magnetic phase transition of (ChTM-TTP)$_2$Au(CN)$_2$ had been originally considered to be the spin-Peierls transition owing to the high transition temperature and the slight broadening of the ESR linewidth, the results presented here support the antiferromagnetic transitions. The present (ChTM-TTP)$_2X$ salts construct a new series of organic conductors that resemble the Bechgaard salts in many respects, while the antiferromagnetic transition temperatures are more than twice as high. This is an important result because many superconducting phases of organic conductors appear next to antiferromagnetic phases, and the superconductivity is considered to be mediated by magnetic fluctuation.[11]

Experimental

Preparation. ChTM-TTP was prepared as described in Refs. 8 and 10. Crystals were grown by electrocrystallization in THF in the presence of the donor and the tetrabutylammonium or tetraethylammonium salts of the corresponding anions under a constant current of 0.2–0.5 μA at 50 °C.

Structure Determination. The crystal structures were determined by the X-ray single crystal structure analyses. All measurements were made on a Rigaku Raxis II area detector with graphite monochromated Mo-$K\alpha$ radiation. The structure of the $AuBr_2^-$ salt was solved by the heavy atom method and was refined by the full-matrix least-squares procedure. For the other salts, the structures were solved by the direct method (SIR88 for the $GaCl_4^-$ salt[12] and SHELX86 for the ReO_4^- salt[13]). Neutral atom scattering factors were taken from Ref. 14. Anisotropic thermal parameters were adopted for all non-hydrogen atoms. Crystallographic data have been deposited at the CCDC, 12 Union Road, Cambridge CB2 1EZ, UK and copies can be obtained on request, free of charge, by quoting the publication citation and the deposition numbers 174688–174692, and the final atomic parameters and structure factors have been deposited as Document No. 75011 at the Office of the Editor of Bull. Chem. Soc. Jpn. From the results of the X-ray crystal structure analyses, the electronic structures were calculated on the basis of the extended Hückel method.[15]

Physical Properties. Electrical resistivities were measured by the four- or two-probe method using low-frequency ac current (typically 10 μA). The high pressure resistivity measurements of the $AuBr_2^-$ salt were carried out by the conventional clamp cell technique. Because about 3 kbar of the pressure is released between room temperature and 77 K, this value has been subtracted from room temperature values.

Electron spin resonance spectra were measured with a conventional X-band spectrometer (JEOL JES-TE100) for the $AuBr_2^-$ and the $GaCl_4^-$ salts. The scan width of the magnetic field was calibrated by the spectra of Mn^{2+}/MgO. The g-values were calibrated by Li-TCNQ (TCNQ: 7,7,8,8-tetracyano-*p*-quinodimethane, $g = 2.0026$). The measurements were carried out for a single crystal. The static magnetic susceptibility of the $AuBr_2^-$ salt was measured by a SQUID magnetometer under the magnetic field of $H = 50$ kOe. The measurements were carried out for aligned crystals (0.615 mg) under the fields of $H \,//\, a$ and $H \,//\, c^*$.

The temperature dependence of the lattice parameters of the $AuBr_2^-$ and the $Au(CN)_2^-$ salts was measured by the imaging plate (DIP320S, MAC Science Co., Inc) equipped with a closed-cycle helium refrigerator (V202C5LZR, DAIKIN Co.), using graphite monochromated Mo-$K\alpha$ radiation. A single crystal was mounted with carbon paste on a copper (for the $AuBr_2^-$ salt) or sapphire (for the $Au(CN)_2^-$ salt) rod attached to a copper cold finger of the closed-cycle refrigerator. Low-temperature crystal structure analyses were carried out for (ChTM-TTP)$_2$AuBr$_2$ at 15.5 K and for (ChTM-TTP)$_2$Au(CN)$_2$ at 9.5 K. The structure was solved by the direct method (SIR88)[12] and refined by the full-matrix least-squares procedure. Neutral atom scattering factors were taken from International Tables.[14] Anisotropic thermal parameters were adopted for all non-hydrogen atoms. The low-temperature electronic structure was also calculated on the extended Hückel method.[15]

Results

Crystal Structures. Crystallographic data of (ChTM-TTP)$_2$AuBr$_2$ are listed in Table 1. The lattice constants show that the $AuBr_2^-$ and the $Au(CN)_2^-$ salts are isostructual.[8] The volume of the unit cell of the present compound is larger than that of the $Au(CN)_2^-$ salt (1271(5) Å^3). The same trend has been observed in BEDT-TTF salts; the unit cell volume of α'-(BEDT-TTF)$_2$AuBr$_2$ is larger than that of α'-(BEDT-TTF)$_2$Au(CN)$_2$.[16] A unit cell contains two donor molecules and one anion; a whole donor molecule is crystallographically independent, and located on a general position, and an anion is located on an inversion center similarly to (ChTM-TTP)$_2$Au(CN)$_2$. The refinement of the anion population shows no deficiency. Therefore 2:1 composition is concluded from the structure.

Table 1. Crystallographic Data

	(ChTM-TTP)$_2$AuBr$_2$	(ChTM-TTP)$_2$AuBr$_2$	(ChTM-TTP)$_2$Au(CN)$_2$	(ChTM-TTP)$_2$GaCl$_4$	(ChTM-TTP)ReO$_4$
Chemical formula	$C_{36}H_{32}AuBr_2S_{24}$	$C_{36}H_{32}AuBr_2S_{24}$	$C_{38}H_{32}AuN_2S_{24}$	$C_{36}H_{32}Cl_4GaS_{24}$	$C_{18}H_{16}O_4ReS_{12}$
Formula weight	1591.01	1591.01	1483.2	1445.8	867.32
Shape	Black thin plate	Black thin plate	Black thin plate	Black thin plate	Black plate
Crystal system	Triclinic	Triclinic	Triclinic	Triclinic	Triclinic
Space group	$P\bar{1}$	$P\bar{1}$	$P\bar{1}$	$P\bar{1}$	$P\bar{1}$
a / Å	9.77(1)	9.599(3)	9.5950(8)	9.48(2)	13.131(6)
b / Å	17.41(2)	17.029(6)	17.210(1)	17.25(1)	14.030(5)
c / Å	8.977(6)	8.765(4)	8.7830(8)	9.39(1)	7.971(1)
α / °	98.09(5)	97.21(2)	97.834(7)	90.86(8)	97.18(2)
β / °	116.27(5)	115.58(3)	115.543(6)	117.4(1)	102.17(2)
γ / °	74.50(7)	74.90(2)	73.811(5)	95.9(1)	104.70(4)
V / Å^3	1318(2)	1247.5(9)	1256.5(2)	1351(3)	1363.5(9)
Z	1	1	1	1	2
D_{calc} / g cm^{-3}	2.005	2.117	1.960	1.776	2.112
λ/ Å	0.71070	0.71070	0.71070	0.71070	0.71070
Temperature / K	293	15.5	9.5	293	270
μ (Mo-$K\alpha$) / mm^{-1}	5.233	5.602	3.971	1.631	5.428
R	0.100	0.083	0.075	0.115	0.062
R_w[a)]	0.106	0.110	0.112	0.112	0.069
Goodness of fit	2.520	2.648	3.284	0.560	1.040
Reflections used	1864 ($I > 5.0\ \sigma(I)$)	2796 ($I > 3.0\ \sigma(I)$)	4449 ($I > 3.0\ \sigma(I)$)	1727 ($I > 3.0\ \sigma(I)$)	4915 ($I > 3.0\ \sigma(I)$)

a) $w = 1/\sigma(I)^2$

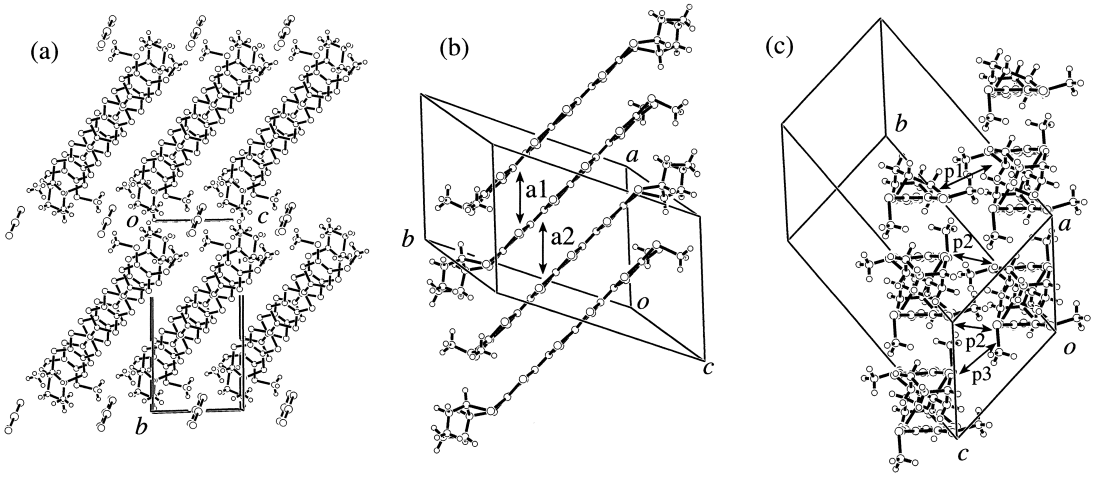

Fig. 1. Crystal structure of (ChTM-TTP)$_2$AuBr$_2$. (a) Projection onto the *bc* plane, (b) view along the molecular short axis, and (c) view along the molecular long axis.

Although the donor molecules form the layers separated by anion layers like (TMT*C*F)$_2X$ (Fig. 1(a)), the cyclohexane rings are incorporated in the anion layers, and construct the insulating layer together with the anions. The donor molecules are stacked along the *a* axis (Fig. 1(b)). Figure 2 shows the overlap modes in the stack. Because the donor molecules dimerize along the stacking direction, there are two overlap modes. Both modes are ring-over-bond type. In one overlap mode named a1 (Figs. 1(b) and 2), the slip distance[17] along the molecular long axis (D_{a1}) is 1.83 Å, which corresponds to about a half of the length of a 1,3-dithiole ring. The interplanar distance of the a1 mode (Z_{a1}) is 3.53 Å. The other overlap mode named a2 (Figs. 1(b) and 2) is the same as the uniform overlapping mode in (TTM-TTP)I$_3$ (TTM-TTP: 2,5-bis[4,5-bis(methylthio)-1,3-dithiol-2-ylidene]-1,3,4,6-tetrathiapentalene); the slip along the molecular long axis of a2 (D_{a2}) is 4.88 Å, which corresponds to one and a half lengths of a 1,3-dithiole ring.[18] The interplanar distance of a2 (Z_{a2}) is 3.57 Å. This is slightly larger than that of the a1 mode.

Crystallographic data of (ChTM-TTP)$_2$GaCl$_4$ are listed in Table 1. The lattice constants show that the $GaCl_4^-$ and the $AuBr_2^-$ salts are not isostructual. The volume of a unit cell of the $GaCl_4^-$ salt is larger than that of the $AuBr_2^-$ salt. A unit cell contains two donor molecules and one anion; a whole donor molecule is crystallographically independent, and located on a general position. The Ga atom is slightly displaced from an inversion center, so that there is a disorder in the anions. Since the Ga atom site is occupied with 50% probability, the composition is 2:1. This disorder is not the same as that of (TMTSF)$_2$ClO$_4$; the Cl atoms in (TMTSF)$_2$ClO$_4$ are located on

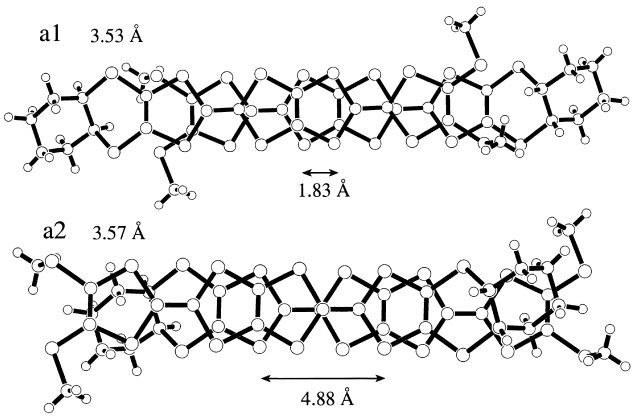

Fig. 2. Overlap modes of intrastack interactions in (ChTM-TTP)$_2$AuBr$_2$.

an inversion center and the oxygen atoms randomly occupy eight nearly equivalent positions.[19]

The donor molecules are stacked along the *a* axis (Fig. 3). The structure of the donor chain is basically the same as for the $AuBr_2^-$ and $Au(CN)_2^-$ salts. Because the donor molecules dimerize along the stacking direction, there are two overlap modes. Both modes are ring-over-bond type. In one overlap mode named a1 (Fig. 3(b)), the slip distance D_{a1} is 1.66 Å. This is shorter than that of the $AuBr_2^-$ salt. The interplanar distance Z_{a1}, 3.46 Å, is also shorter than the $AuBr_2^-$ salt (3.53 Å). In another overlap mode named a2 (Fig. 3(b)) the slip distance D_{a2} is 4.75 Å. The interplanar distance Z_{a2}, 3.53 Å, is the same as for the a1 mode of the $AuBr_2^-$ salt. These short interplanar and the slip distances are consistent with the length of the *a* axis being shorter than that of the $AuBr_2^-$ salt, because the inclination of the donor molecules from the stacking axis is almost the same as that for the $AuBr_2^-$ salt.

Crystallographic data of (ChTM-TTP)ReO_4 are also listed in Table 1. The ORTEP drawing and the atomic numbering scheme of the ReO_4^- salt are shown in Fig. 4. The lattice constants indicate that the ReO_4^- salt is not isostructural to either the $AuBr_2^-$ or the $GaCl_4^-$ salts. Two donor molecules and two anions are contained in a unit cell in the ReO_4^- salt. One donor molecule and one anion are located on general positions (Fig. 5(a)), then the donor to anion ratio is 1:1 and there is no anion disorder in (ChTM-TTP)ReO_4.

Although the donor molecules form the layers separated by anion layers like the Bechgaard salts, the anion layer is not obvious because the ReO_4^- anions are located on the side of the 1,2-cyclohexylenedithio rings (Fig. 5(a)). The donor molecules are stacked along the *b* axis (Figs. 5(b) and 5(c)). Because the donor molecules dimerize along the stacking direction, there are two overlap modes in the stack. Both modes are ring-over-bond type, but are largely different from the other three ($AuBr_2$, $Au(CN)_2$, and $GaCl_4$) salts. The interplanar distances are 3.46 Å for the Z_{b1} and 3.54 Å for the Z_{b2}. The slip distances are 4.53 Å for the D_{b1} and 7.63 Å for the D_{b2} (Fig. 6). These slip distances are considerably larger than the other three salts (typically 1.8 and 4.8 Å), indicating a reduced intrachain interaction and an enhanced dimerization.

Energy Band Structures. Calculated intermolecular overlap integrals of the HOMO and the molecular arrangements of three kinds of compounds are listed in Table 2. All overlap modes are shown in Figs. 1, 3, and 5. The difference between S_{a1} (S_{b1} for the ReO_4^- salt) and S_{a2} (S_{b2} for the ReO_4^- salt) designates the degree of dimerization along the stack. When $S_{a2}/S_{a1} = 1$, the system has a uniform structure. The strong dimerization makes this parameter close to zero. The value of S_{a2}/S_{a1} is 0.76 for the $AuBr_2^-$ salt (bottom of Table 2), then the dimerization is a little weaker than that of the $Au(CN)_2^-$ salt, where the ratio is 0.70.[8] On the other hand, the ratio is 0.53 for the $GaCl_4^-$ salt and 0.33 for the ReO_4^- salt. These values are much smaller than that of the $AuBr_2^-$ salt. Therefore, the tetrahedral anions make the strongly dimerized structures.

For (ChTM-TTP)$_2$AuBr$_2$, the intrastack overlaps are ten times as large as those of the interstack overlaps (Table 2). The side by side interactions along the molecular short axis are small. The transverse interactions are, however, larger than

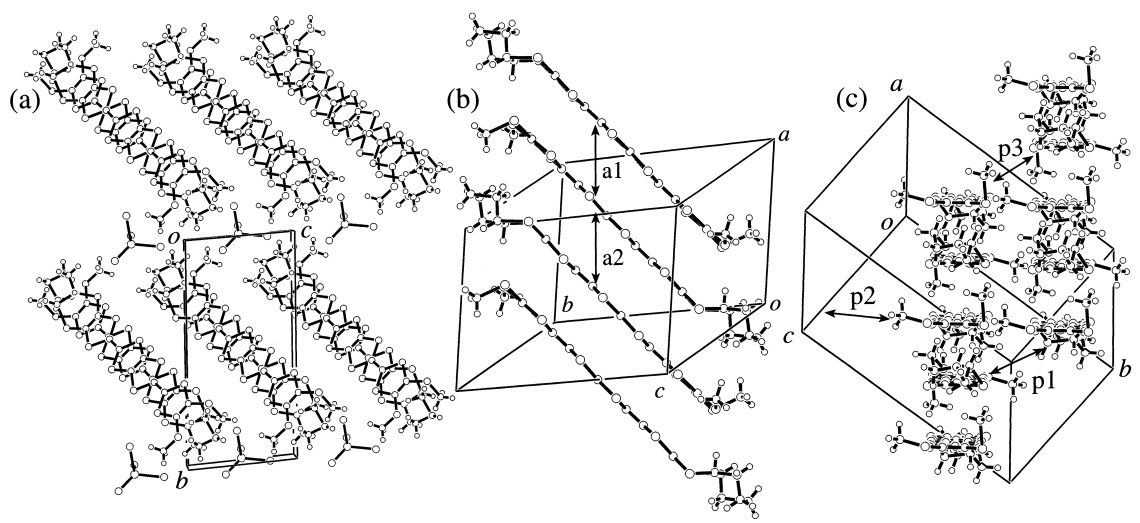

Fig. 3. Crystal structure of (ChTM-TTP)$_2$GaCl$_4$. (a) Projection onto the *bc* plane, (b) view along the molecular short axis, and (c) view along the molecular long axis.

Table 2. Intermolecular Overlap Integrals, S ($\times 10^{-3}$) of HOMO, and the Molecular Arrangements of (ChTM-TTP)$_2$AuBr$_2$, (ChTM-TTP)$_2$Au(CN)$_2$, (ChTM-TTP)$_2$GaCl$_4$, and (ChTM-TTP)ReO$_4$. D, Z, and L Denote the Slip Distance along the Molecular Long Axis, the Interplanar Distance, and the Distance between the Center of the TTP Unit

	$AuBr_2$ (293 K)	$AuBr_2$ (15.5 K)	$Au(CN)_2$ (293 K)	$Au(CN)_2$ (9.5 K)	$GaCl_4$ (293 K)	ReO_4 (270 K)
S_{a1} (S_{b1})	9.31	11.33	11.27	12.56	14.65	14.99
D_{a1} / Å	1.83	1.83	1.87	1.81	1.66	4.53
Z_{a1} / Å	3.53	3.42	3.50	3.45	3.46	3.46
S_{a2} (S_{b2})	7.09	8.94	7.89	8.77	7.70	4.99
D_{a2} / Å	4.88	4.86	4.94	4.85	4.75	7.63
Z_{a2} / Å	3.57	3.47	3.50	3.47	3.53	3.54
S_{p1}	1.48	1.83	1.24	1.64	0.61	−1.78
ϕ_{p1}	23.7°	24.0°	26.0°	24.1°	29.1°	2.9°
D_{p1} / Å	5.88	5.81	5.76	5.84	5.92	7.72
L_{p1} / Å	8.93	8.81	8.80	8.84	9.21	9.94
S_{p2}	1.27	1.47	1.77	1.60	2.14	−0.27
ϕ_{p2}	7.5°	6.8°	5.5°	6.8°	0.3°	2.1°
D_{p2} / Å	7.71	7.64	7.63	7.65	7.58	10.8
L_{p2} / Å	9.92	9.81	9.79	9.82	9.80	12.6
S_{p3}	1.15	1.47	1.55	1.64	0.52	−0.37
ϕ_{p3}	23.3°	23.7°	25.1°	23.7°	29.2°	31.1°
D_{p3} / Å	2.83	2.79	2.69	2.80	2.83	3.19
L_{p3} / Å	7.50	7.35	7.36	7.36	7.70	7.97
S_{a2}/S_{a1}	0.76	0.79	0.70	0.70	0.53	0.33

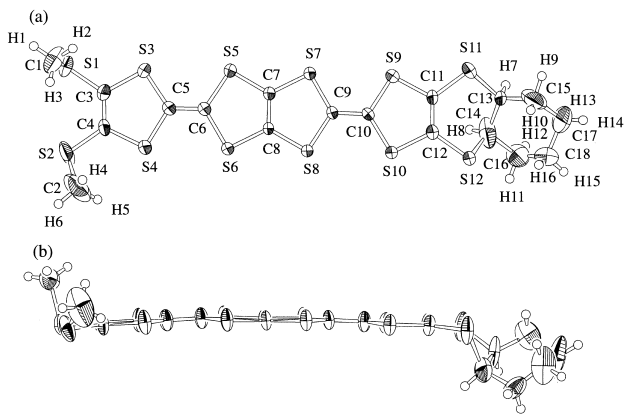

Fig. 4. (a) ORTEP drawing and atomic numbering scheme of the donor molecule of (ChTM-TTP)ReO_4 and (b) side view of the donor molecule of (ChTM-TTP)ReO_4.

those of (TTM-TTP)I_3, (TTM-TTP)$(I_3)_{5/3}$, and (TSM-TTP)$(I_3)_{5/3}$ (TSM-TTP: 2,5-bis[4,5-bis(methylseleno)-1,3-dithiol-2-ylidene]-1,3,4,6-tetrathiapentalene).[20–23] This situation has a close resemblance to (ChTM-TTP)$_2$Au(CN)$_2$. Therefore the electronic structure of the $AuBr_2^-$ salt is regarded as quasi-one-dimensional. Figure 7(a) shows the energy band structure of (ChTM-TTP)$_2$AuBr$_2$ calculated on the basis of the extended Hückel orbital calculation and the tight-binding method. Because the unit cell contains two donor molecules, there are two branches of the energy band. The Fermi surface of (ChTM-TTP)$_2$AuBr$_2$ is open and the shape is similar to that of the Bechgaard salts.

For (ChTM-TTP)$_2$GaCl$_4$, the intrastack overlaps are about ten times as large as those of the interstack overlaps, except for the p2 mode (S_{p2} in Table 2). It is clear that the dimerization gap (the gap between the upper and the lower energy band) is larger than that of the $AuBr_2^-$ salt, as shown in Fig. 7(b). The Fermi surface of (ChTM-TTP)$_2$GaCl$_4$ is open and corrugated (Fig. 7(b)).

For (ChTM-TTP)ReO_4, the side-by-side interaction is smaller than that of the $GaCl_4^-$ salt. Therefore the electronic structure of this compound is regarded as highly one-dimensional. The ReO_4^- salt has an energy gap at the Fermi level owing to the dimerized 1:1 composition like (TTM-TTP)AuI_2.[24] Accordingly, it is expected that this compound will show semiconducting behavior.

Transport Properties. For (ChTM-TTP)$_2$AuBr$_2$, the conductivity at room temperature is about 80 S cm^{-1}. Figure 8(a) shows the temperature dependence of the electrical resistivity of (ChTM-TTP)$_2$AuBr$_2$. The resistivity exhibits almost metal-like behavior below room temperature, and this is in agreement with the energy band calculation. Then the resistivity increases gradually below 150 K and rapidly below 100 K at ambient pressure. It is difficult to specify the metal-insulator transition temperature; this behavior is not a "transition" but a crossover from metallic to insulating region. Several one-dimensional compounds based on the TTP series donors show this kind of crossover.[22,23] A slight applied pressure leads to a clear metallic state in the high temperature region, where the resistivity decreases as the temperature decreases (inset of Fig. 8(a)). Al-

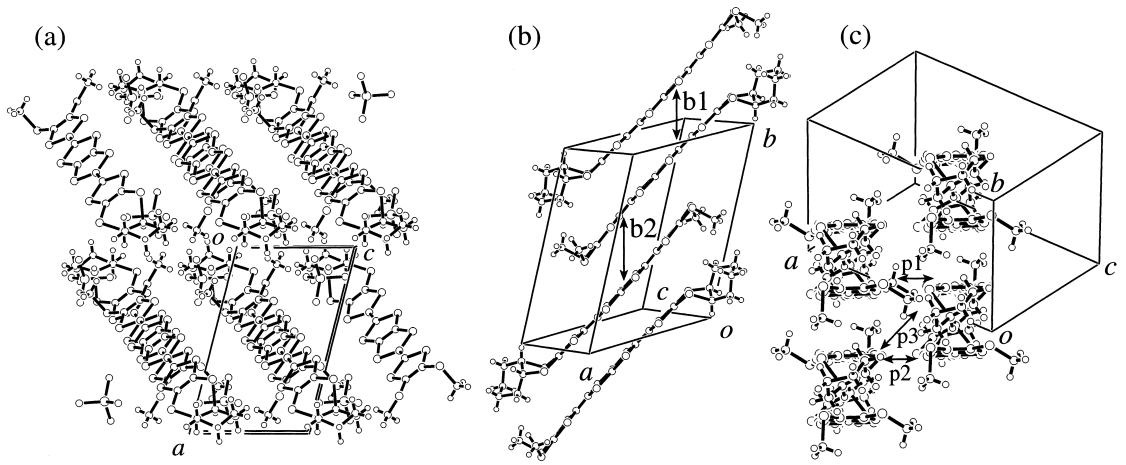

Fig. 5. Crystal structure of (ChTM-TTP)ReO_4. (a) Projection onto the *ac* plane, (b) view along the molecular short axis, and (c) view along the molecular long axis.

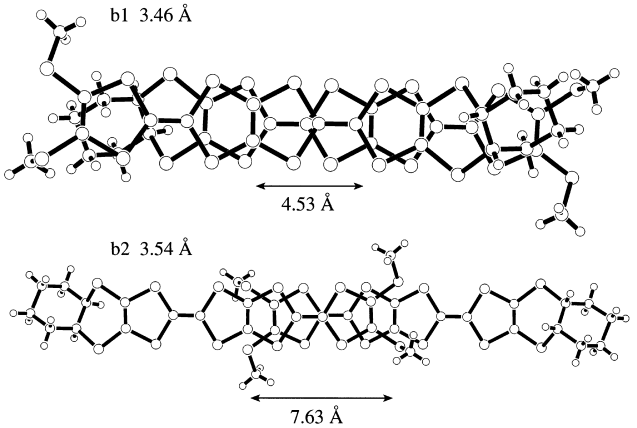

Fig. 6. Overlap modes of intrastack interactions in (ChTM-TTP)ReO_4.

though the charge localization temperature shifts to lower temperatures as the pressure increases, the insulating phase is not completely suppressed even at 9.0 kbar.

Thermoelectric power (Seebeck coefficient) of (ChTM-TTP)$_2$AuBr$_2$ was measured as shown in Fig. 8(a). The room-temperature value is 22 μV/K (25 μV/K for the Au(CN)$_2^-$ salt[9]), and we can estimate the bandwidth to be 0.91 eV (0.80 eV for the Au(CN)$_2^-$ salt) using the one-dimensional tight-binding approximation.[25] This value is close to those of the Bechgaard salts (1.0 eV).[26]

The tight-binding band of a dimerized chain shown in Fig. 9 is expressed by

$$E(k) = \pm\sqrt{t_1^2 + t_2^2 + 2t_1t_2\cos(ka)}, \quad (1)$$

where t_1 is the transfer integral within the dimerized unit, t_2 is that between the dimerized units, and a is the periodicity of the dimerized unit along the stacking axis. The upper band given by Eq. 1 is half filled in the crystal of (ChTM-TTP)$_2$AuBr$_2$, so that this energy band leads to a metallic behavior. We can estimate the transfer integrals and the dimerization gap by using the bandwidth estimated from the thermoelectric power, when

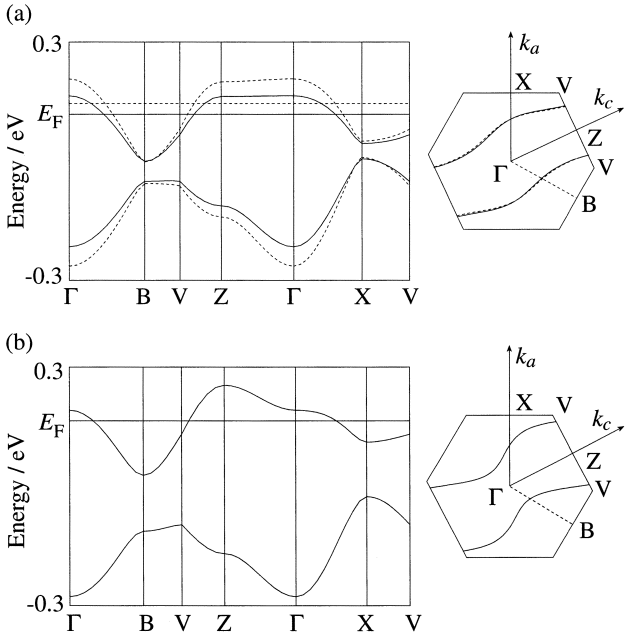

Fig. 7. Tight-binding energy band structure and the Fermi surface of (a) (ChTM-TTP)$_2$AuBr$_2$ and (b) (ChTM-TTP)$_2$GaCl$_4$ calculated from the overlap of the HOMO obtained on the basis of the extended Hückel molecular orbital calculation (Table 2). The dotted lines of (a) are calculated by using the crystal data at 15.5 K.

we assume that the ratio of the transfer integrals, t_2/t_1, is equal to the ratio of the overlap integrals, $S_{a2}/S_{a1} = 0.76$, as given in the previous section. The estimated transfer integrals are $t_1 = 0.25$ eV and $t_2 = 0.19$ eV, and the dimerization gap, $\Delta_D = 2(t_1 - t_2)$, is 0.12 eV. For the Au(CN)$_2^-$ salt, the parameters are $t_1 = 0.23$ eV, $t_2 = 0.16$ eV, and $\Delta_D = 0.14$ eV.

The thermoelectric power of (ChTM-TTP)$_2$AuBr$_2$ linearly decreases as the temperature decreases, and gradually goes to the negative range below 100 K. This behavior indicates that charge localization occurs below 100 K. Moreover, the thermopower goes to zero below 25 K. A similar anomaly has

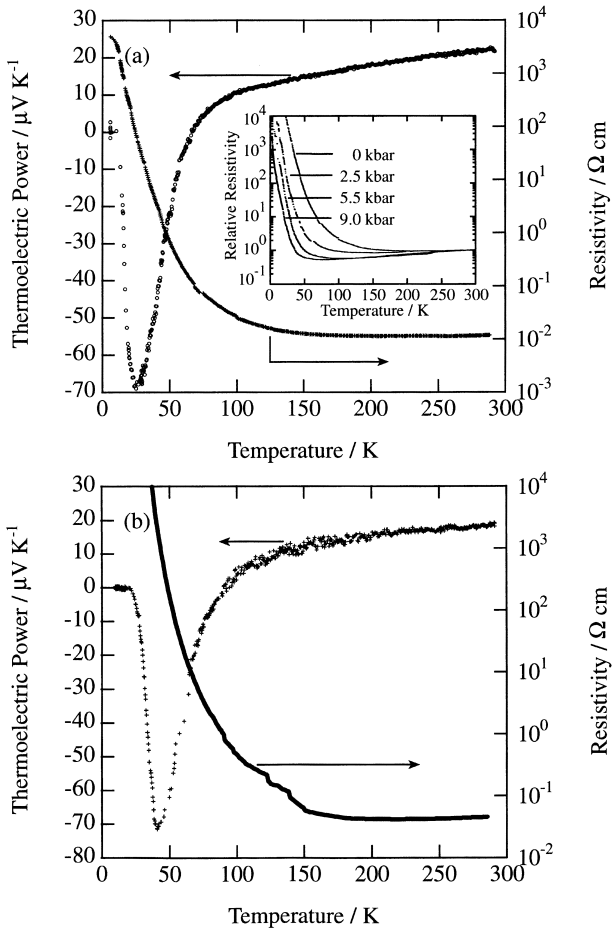

Fig. 8. Temperature dependence of electrical resistivity and thermoelectric power of (a) (ChTM-TTP)$_2$AuBr$_2$ and (b) (ChTM-TTP)$_2$GaCl$_4$. The inset figure in (a) is the temperature dependence of electrical resistivity under various pressures normalized at room temperature.

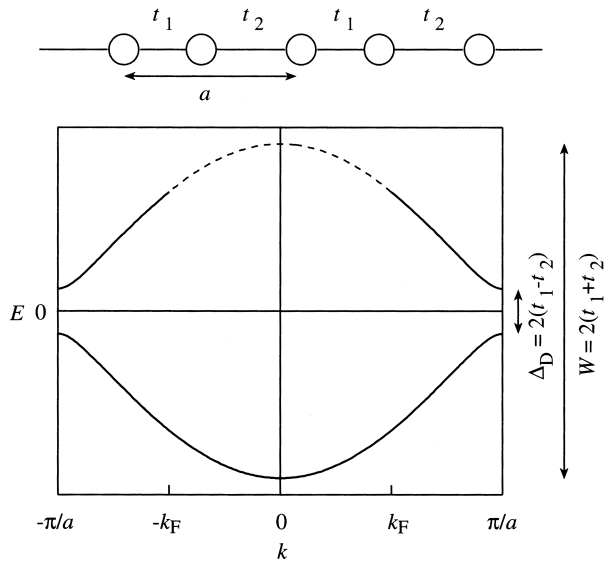

Fig. 9. Schematic energy band of one-dimensional dimerized chain. The solid and dashed lines denote the occupied and unoccupied bands, respectively.

been observed in (DIMET)$_2$I$_3$ (DIMET: 4,5-(ethylenedithio)-4′,5′-dimethyl-1,1′,3,3′-tetrathiafulvalene).[27] In this case, Saito et al. have pointed out that this anomaly appears around the temperature where the activation energy of the resistivity shows an anomaly. In (ChTM-TTP)$_2$AuBr$_2$, however, the resistivity does not show any clear anomaly around 25 K.

For (ChTM-TTP)$_2$GaCl$_4$, the conductivity at room temperature is about 20 S cm^{-1}. Figure 8(b) shows the temperature dependence of electrical resistivity of (ChTM-TTP)$_2$GaCl$_4$ at ambient pressure. This salt shows metallic behavior around room temperature, and then the resistivity rapidly increases below 150 K.

Thermoelectric power (Seebeck coefficient) of (ChTM-TTP)$_2$GaCl$_4$ is also shown in Fig. 8(b). The room-temperature value is 19 μV/K, from which we can estimate the bandwidth to be 1.05 eV by using the one-dimensional tight-binding approximation. The estimated transfer integrals are $t_1 = 0.34$ eV and $t_2 = 0.18$ eV, and the dimerization gap, Δ_D, is 0.32 eV. This dimerization gap is twice as large as those of other (ChTM-TTP)$_2X$ salts. The thermoelectric power linearly decreases as the temperature decreases, and gradually goes to the negative range below 150 K. The behavior of both the resistivity and the thermopower indicates that the charge localization occurs below 150 K. The thermoelectric power shows the same type of anomalous behavior as that of the $AuBr_2^-$ salt at 40 K.

For (ChTM-TTP)ReO$_4$, the room temperature conductivity is about 8×10^{-3} S cm^{-1}.[28] (ChTM-TTP)ReO$_4$ shows semiconducting behavior below room temperature and the activation energy is about 0.14 eV. This activation energy is four times as large as that of (TTM-TTP)AuI$_2$.[24]

Magnetic Properties. Figure 10 shows the angle dependence of ESR peak-to-peak linewidths and the g-values of (ChTM-TTP)$_2$AuBr$_2$ at room temperature. The ESR line shape is a single Lorentzian. Because the donor molecules are largely tilted with respect to the stacking axis (43.4°) as shown in Figs. 1 and 10, the linewidth and g-value attain peaks in the corresponding oblique direction (about $\theta \approx 46°$ from the b^* axis). We also rotated the magnetic field in the molecular plane (ϕ) and around the molecular plane (ω) to determine the principal g-values. Because the molecular long axis is a little tilted with respect to the b^* axis as shown in Fig. 1, the maximum g-value appears at $\phi \approx 165°$ in Fig. 10. Although the minimum g-value appears at $\omega \approx 150°$, the reason is the same as that of the maximum g-value. The principal g-values are determined by a fitting to the equation:

$$g^* = \sqrt{g_i^2 \cos^2\theta + g_j^2 \sin^2\theta}, \quad (2)$$

where g^* is the observed g-value, g_i and g_j are the principal g-values, and θ is the angle. The observed peak-to-peak linewidths, ΔH^*, were also fitted with an analogous equation:

$$\Delta H^* = \Delta H_i \cos^2\theta + \Delta H_j \sin^2\theta. \quad (3)$$

The principal g-values are determined from the $g(\phi)$ and $g(\omega)$ curves. The estimated principal g-values are $g_{max} = 2.0093$, $g_{mid} = 2.0050$, and $g_{min} = 2.0016$. The linewidth is broad and nearly constant when $\boldsymbol{H}$ is on the molecular plane ($\Delta H_{pp}(\phi)$

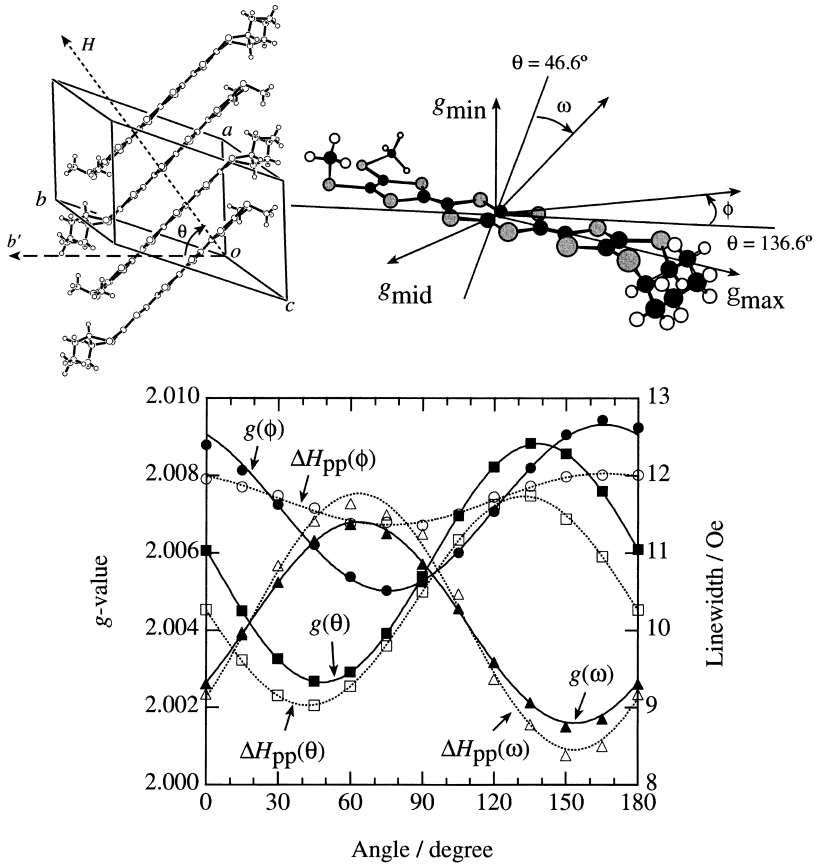

Fig. 10. Angle dependence of the ESR linewidths (open symbols) and the g-values (closed symbols) of (ChTM-TTP)$_2$AuBr$_2$ at room temperature. The solid and dotted lines are fit to the Eqs. 2 and 3, respectively. The upper pictures show the definition of the rotation angles θ, ϕ, and ω.

curve in Fig. 10), while it is narrow when $\boldsymbol{H}$ is applied normal to the plane. Such linewidth behavior has been also observed in β-(BEDT-TTF)$_2X$ (X = I_3 and IBr_2).[29] In the obtained principal g-values, g_{max} and g_{mid} are smaller than those of TMTTF[30] and BEDT-TTF[4] salts. On the other hand, g_{min} is close to the value of the free electron.

Although the narrow linewidth at room temperature means high one-dimensionality, the linewidth of (ChTM-TTP)$_2$AuBr$_2$ is twice as large as that of (TMTTF)$_2X$ (X = ClO_4, PF_6, BF_4, SCN, Br).[30,31] The g-shift is smaller than that of the TMTSF salts, due to the difference between sulfur and selenium atoms in spin-orbital couplings.[30,32]

For (ChTM-TTP)$_2$AuBr$_2$, the temperature dependence of the ESR linewidth and the normalized spin susceptibility is shown in Fig. 11. The g-value is almost constant, but shows a small increase below 15 K. The ESR linewidth (H // b^*) becomes narrow as the temperature decreases, and exhibits a slight broadening below 26 K. The broadening of linewidth in the other direction (H // a) is divergent. The spin susceptibilities of both a- and b^*- axis directions decrease as the temperature decreases. This may be due to a fluctuation in the one-dimensional system, similarly to the (TMT*C*F)$_2X$ salts.[33] The spin susceptibility of (ChTM-TTP)$_2$AuBr$_2$ has no anomaly around 100 K, at which the resistivity and the thermoelectric power show the crossover to the insulating state. If the charge localization is associated with the CDW or the SDW transitions, a decrease of the spin susceptibility is expected at this temperature ($\approx$ 100 K). Therefore the possibilities of the density-wave transitions as the origin of the charge localization will be eliminated. The spin susceptibility, however, rapidly decreases below 37 K. The ESR signal could not be detected at liquid He temperatures. The linewidth shows a small broadening below 26 K, but the broadening is too small to be undoubtedly attributed to an antiferromagnetic transition.

Figure 12 shows the temperature dependence of static magnetic susceptibility under 50 kOe measured for aligned crystals. The susceptibility is almost constant from room temperature to 50 K, and can be regarded as the Pauli paramagnetism. Although the susceptibility parallel to the a axis (χ_a) is almost constant below 50 K, χ_{c^*} rapidly decreases below 38 K. This anisotropic behavior demonstrates that the magnetic phase transition is not the spin-Peierls transition but the antiferromagnetic phase transition at $T_N \approx 38$ K.

The magnetization has not been saturated up to 50 kOe in the magnetic field dependence of the magnetization at either room temperature or 4 K. The flop field of many organic conductors is below 10 kOe: 4.5 kOe for (TMTSF)$_2$AsF$_6$ and 4.2 kOe for (TMTTF)$_2$Br.[34,35] However, recently spin-flop in (DMET)$_2$FeBr$_4$ (DMET: 4,5-(ethylenedithio)-4′,5′-dimethyl-1′,3′-diselena-1,3-dithiafulvalene, $T_N \approx 3.7$ K) has been found at H = 20 kOe.[36] A high spin flop field means that the anisotropy and the exchange fields are much larger than those of the

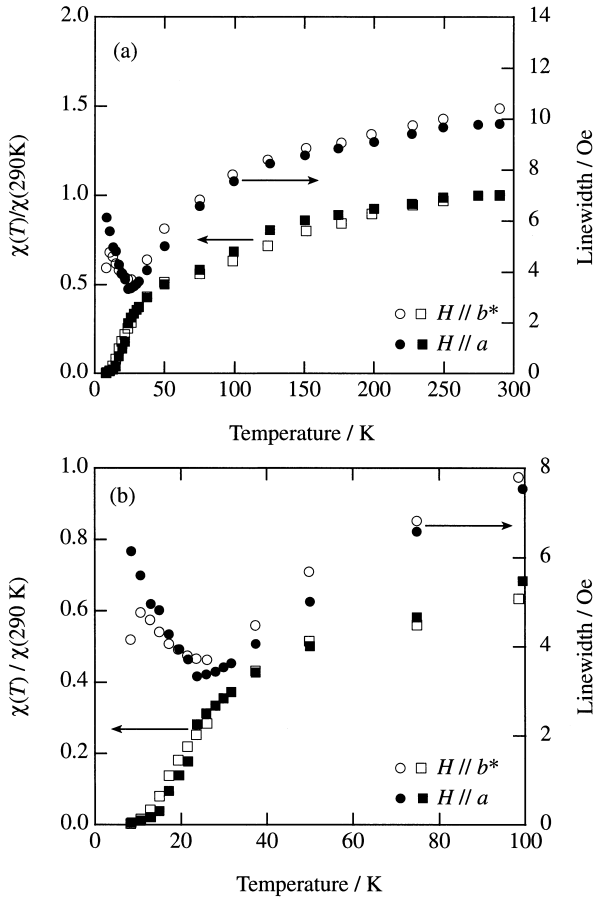

Fig. 11. Temperature dependence of ESR linewidths and the relative spin susceptibilities of $(ChTM\text{-}TTP)_2AuBr_2$ (H // b^* and H // a) in the measurement temperature range (a) and in the low temperature region (b).

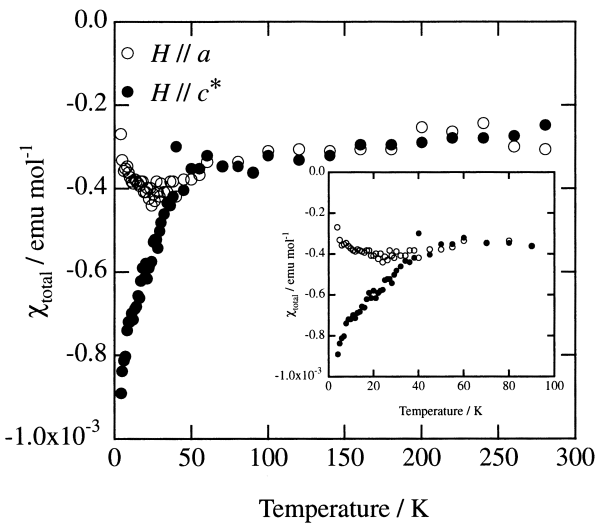

Fig. 12. Temperature dependence of static magnetic susceptibility of $(ChTM\text{-}TTP)_2AuBr_2$ under H = 50 kOe, measured for aligned crystals (H // a and H // c^*). The inset figure is the low temperature region.

Bechgaard salts.

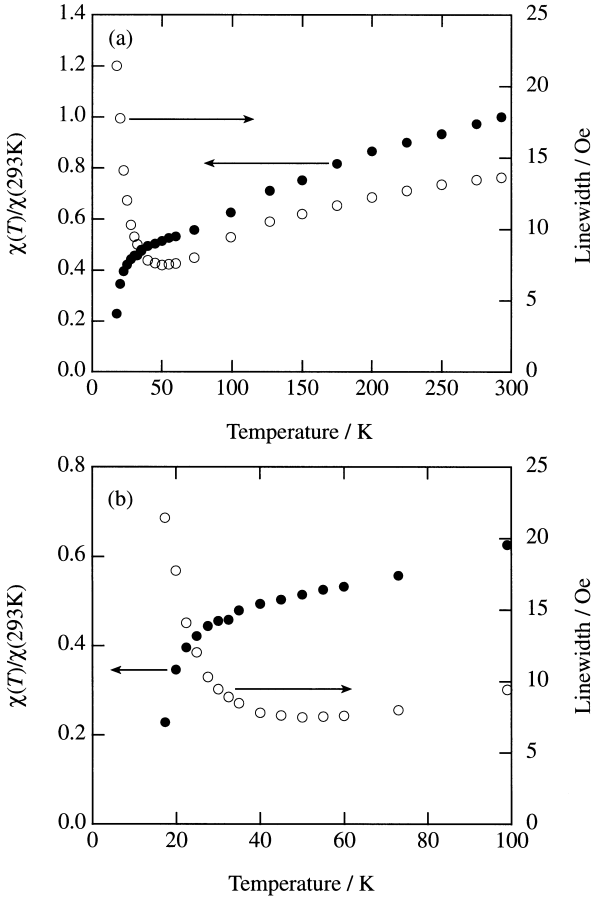

Fig. 13. Temperature dependence of ESR linewidths and the relative spin susceptibilities of $(ChTM\text{-}TTP)_2GaCl_4$ (H // c^*) in the wide temperature range (a) and in the low temperature region (b).

Although these results indicate that the easy axis is the c^* axis, it is not clear that the a axis is the hard axis or the intermediate axis. In $(TMTSF)_2AsF_6$, the easy axis is the b^* axis which is the interstack direction in the conducting plane, and the a axis, the stacking direction, is the intermediate axis.[34] Although the easy axis of $(TMTTF)_2Br$ is the same direction as that of $(TMTSF)_2AsF_6$, the intermediate axis is the c^* direction and the hard axis is the b^* one in spite of the same crystal structure.[35] Therefore, we cannot speculate about the a-axis of $(ChTM\text{-}TTP)_2AuBr_2$. The easy axis of $(ChTM\text{-}TTP)_2AuBr_2$ is, however, oriented in the same direction as both $(TMTSF)_2AsF_6$ and $(TMTTF)_2Br$, that is, along the molecular short axis.

For $(ChTM\text{-}TTP)_2GaCl_4$, Fig. 13 shows the temperature dependence of the ESR linewidth and the normalized spin susceptibility (H // c^*). The g-value of this direction is 2.0072 at room temperature, and shows a small decrease below 50 K and an increase below 25 K. The spin susceptibility decreases as the temperature decreases, presumably because of a spin fluctuation in the one-dimensional system. The spin susceptibility has no anomaly around the charge localization temperature (150 K), and then rapidly decreases below 32 K. These results are similar to those of $(ChTM\text{-}TTP)_2AuBr_2$. Although the ESR linewidth becomes narrow as the temperature decreases,

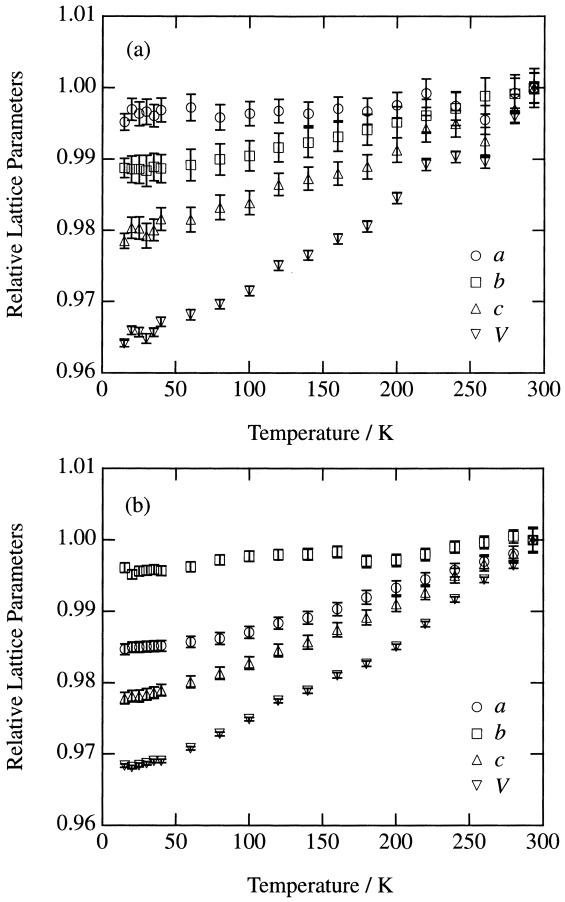

Fig. 14. Temperature dependence of the lattice parameters and the cell volume of (a) (ChTM-TTP)$_2$AuBr$_2$ and (b) (ChTM-TTP)$_2$Au(CN)$_2$ (normalized at 293 K). The unit cell of (ChTM-TTP)$_2$Au(CN)$_2$ is taken similarly to that of (ChTM-TTP)$_2$AuBr$_2$ at room temperatures (see Ref. 8.).

it exhibits a divergent increase below 50 K; the linewidth at 17 K is about three times as large as that at 50 K. This clear divergence of the linewidth is different from that of (ChTM-TTP)$_2$AuBr$_2$. This divergent linewidth indicates an antiferromagnetic phase transition at the Néel temperature, $T_N \approx 32$ K.

Low-Temperature Crystal Structures. The low-temperature X-ray photographs of both (ChTM-TTP)$_2$AuBr$_2$ and (ChTM-TTP)$_2$Au(CN)$_2$ were taken at 15.5 K for 12 h to investigate the existence of the superstructure. The photographs show no superstructure which has the intensity more than 1/500 times of the Bragg reflections. This indicates that the phase transitions observed in the magnetic properties are not the spin-Peierls transition. This supports the conclusion that the magnetic phase transition of (ChTM-TTP)$_2$Au(CN)$_2$ is an antiferromagnetic transition.

Figure 14 shows the temperature dependence of the lattice parameters of (ChTM-TTP)$_2$AuBr$_2$ and (ChTM-TTP)$_2$Au(CN)$_2$. All lattice parameters of both salts show no anomalous behavior over the entire temperature range; this indicates that these salts have no structural phase transition.

Low-temperature crystal structure analyses and the energy band calculations based on the low-temperature crystal structures were carried out. The low-temperature crystallographic data of (ChTM-TTP)AuBr$_2$ and (ChTM-TTP)Au(CN)$_2$ are listed in Table 1. We describe the low-temperature crystal structure of (ChTM-TTP)$_2$AuBr$_2$ only, because there is basically no structural change in both compounds. Most C–S bond lengths are shorter than those at room temperature, and C=C bond lengths connecting 1,3-dithiole rings do not change for (ChTM-TTP)$_2$AuBr$_2$. The interplanar and the slip distances along the molecular long axis of the a1 mode are 3.42 Å and 1.83 Å, respectively (Table 2). For the a2 mode, the interplanar distance is 3.47 Å and the slip distance is 4.86 Å. The differences of the interplanar distances between room and low temperatures are larger than those of the slip distances.

Calculated intermolecular overlap integrals of the HOMO are listed in Table 2. The ratio of the overlap integrals along the stacking direction (S_{a2}/S_{a1}) is 0.79 for the $AuBr_2^-$ salt and 0.70 for the $Au(CN)_2^-$ salt. The dimerization of these compounds is almost the same as that at room temperature. The shape of the Fermi surface of these salts does not change, as shown in Fig. 7.

Discussion

As for the molecular structure of both (ChTM-TTP)$_2$AuBr$_2$ and (ChTM-TTP)$_2$GaCl$_4$, one methylthio group of ChTM-TTP is located on the molecular plane defined by the two TTF groups, though another one extends out of this plane. This structure is consistent with the partially oxidized donor. It has been observed that all methylthio groups are located on the molecular plane in TTM-TTP$^+$ like (TTM-TTP)X (X = I_3, AuI_2, and $AuBr_2$)[18,24] and in neutral TTM-TTP all methylthio groups are out of the plane.[37] For (ChTM-TTP)ReO_4, it is expected that two methylthio groups of the ChTM-TTP molecule are located in the molecular plane, because of the ChTM-TTP molecule with high oxidation state +1. In the present case, however, one methylthio group is located in the molecular plane, while another one extends out of this plane like other (ChTM-TTP)$_2X$ (Fig. 4). A similar exception has been, however, observed in (TTM-TTP)[C(CN)$_3$].[38]

The 1,2-cyclohexylenedithio ring considerably deviates from the molecular plane (Fig. 4(b)). The bend of the ethylenedithio ring of ChTM-TTP is much larger than that of BEDT-TTF salts or BEDT-TTP (BEDT-TTP: 2,5-bis(4,5-ethylenedithio-1,3-dithiol-2-ylidene)-1,3,4,6-tetrathiapentalene) salts.[4,39] Moreover, the bend of the cyclohexane ring of ChTM-TTP is larger than that of CH-TTP (CH-TTP: 2-(4,5-cyclohexeno-1,3-dithiol-2-ylidene)-5-(1,3-dithiol-2-ylidene)-1,3,4,6-tetrathiapentalene) salts.[40] The reason is that the cyclohexane ring of CH-TTP is attached to the 1,3-dithiole ring directly with a C=C bond. Therefore the steric freedom is reduced in comparison with ChTM-TTP.

According to the classification of the donor arrangements in Ref. 5, the difference of the stacking pattern between (TMTSF)$_2X$ and β-(BEDT-TTF)$_2X$ lies in the slip directions along the molecular long directions; in the stack of (TMTSF)$_2X$, the donors slide alternately in the opposite directions, while in β-(BEDT-TTF)$_2X$ the donor molecules are displaced in the same direction. From this viewpoint, the molecular arrangement of (ChTM-TTP)$_2X$ is not the TMTSF type but the β-type.[41] The slip distances are, however, not the same as β-(BEDT-TTF)$_2X$. Although the intradimer and the interdimer

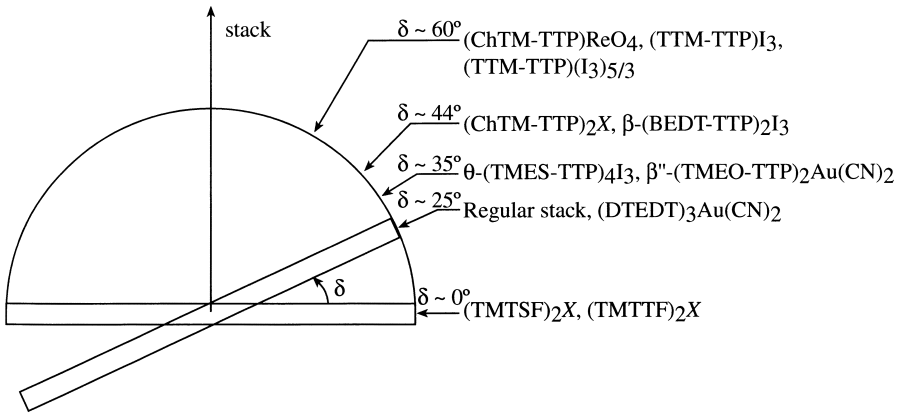

Fig. 15. Inclination of molecular plane δ with respect to the stacking direction. View along the molecular short axis.

Table 3. The Length of the a axis, the Inclination Angle (δ), the Magnitudes of the Dimerization (S_{a2}/S_{a1}), the Charge Localization Temperatures (T_{CL}), and the Néel Temperatures (T_N) of (ChTM-TTP)$_2X$

	a / Å	δ / °	S_{a2}/S_{a1}	T_{CL} / K	T_N / K
(ChTM-TTP)$_2$AuBr$_2$	9.77(1)	43.4	0.76	100	38
(ChTM-TTP)$_2$Au(CN)$_2$	9.76(1)	44.2	0.70	120	(< 40)
(ChTM-TTP)$_2$GaCl$_4$	9.48(2)	42.5	0.53	150	32

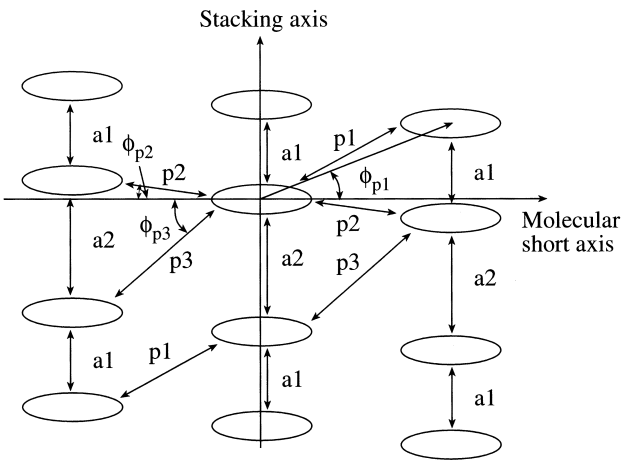

Fig. 16. Schematic donor arrangement and the definition of parameters ai (i = 1, 2), pj (j = 1–3), and ϕ_{pj} (j = 1–3) in (ChTM-TTP)$_2X$ (view along the molecular long axis.). ai , pj, and ϕ_{pj} denote the intrastack overlap mode, the interstack overlap mode, and the angle of the intermolecular vector with respect to the molecular plane.

slip distances are 1.6 Å and 3.8 Å, respectively, for β-(BEDT-TTF)$_2X$, these quantities are 1.66–1.87 Å and 4.75–4.94 Å for (ChTM-TTP)$_2X$.

The inclination of the donor molecule from the stacking direction in (TMTSF)$_2X$ is $\delta = 0°$; this directly comes from the alternating slip. The δ values of several TTP salts are plotted in Fig. 15. Among BEDT-TTF salts, β-(BEDT-TTF)$_2$I$_3$ shows the largest inclination, $\delta = 35°$.[5] (ChTM-TTP)$_2X$ also has a large inclination; for example (ChTM-TTP)$_2$AuBr$_2$ shows δ = 43.4°. In general, TTP series conductors have large inclinations. In this respect, the crystal structure of (ChTM-TTP)$_2X$ is different from that of (TMTSF)$_2X$.

In (ChTM-TTP)$_2X$, the crystal structure of the $GaCl_4^-$ salt is slightly different from those of the $AuBr_2^-$ and the $Au(CN)_2^-$ salts. The interaction (overlap) modes of (ChTM-TTP)$_2X$ are shown in Fig. 16. Table 2 shows the molecular arrangements of (ChTM-TTP)$_2X$: the angle of the p2 mode (ϕ_{p2}) in the $GaCl_4^-$ salt is nearly 0°, which is much smaller than 5–8° of the other salts. This means that in Fig. 3(c) the donor molecule belonging to the adjacent chain, connected by S_{p2}, is located on the same level as the original donor, whereas in the $AuBr_2^-$ salt (Fig. 1(c)), the p2 interaction is tilted by about 6° from the donor plane. This is the reason that the $GaCl_4^-$ salt has similar lattice constants to the other salts, but is not strictly isostructural. Since $\phi = 0°$ corresponds to a maximum of overlap,[5] S_{p2} of the $GaCl_4^-$ salt is much larger than those of the other salts. As for the p1 and p3 modes, the distances between the center of the TTP unit (L_{p1} and L_{p3}) of the $GaCl_4^-$ salt are longer than those of the $AuBr_2^-$ salt. Therefore, overlap integrals of S_{p1} and S_{p3} of the $GaCl_4^-$ salt are smaller than those of the other (ChTM-TTP)$_2X$ salts.

The magnitude of the dimerization parameter, namely the ratio of the interdimer to the intradimer overlap integrals S_{a2}/S_{a1}, indicates that (ChTM-TTP)ReO$_4$ has the strongest dimerization and (ChTM-TTP)$_2$AuBr$_2$ has the weakest one (Table 2). In (TMTSF)$_2X$ (X = ReO$_4$, ClO$_4$, FSO$_3$, NO$_3$, PF$_6$, and AsF$_6$) and (TMTTF)$_2X$ (X = Br, BF$_4$, SCN, ReO$_4$, and PF$_6$), most of the S_{a2}/S_{a1} values are about 0.87–0.98 except (TMTTF)$_2$PF$_6$ (0.68) and (TMTTF)$_2$BF$_4$ (0.74).[42,43] Therefore, the dimerization of the ChTM-TTP salts is stronger than that of the TMT*C*F compounds. In (ChTM-TTP)$_2X$, S_{a2}/S_{a1} is a good parameter that scales the charge localization temperature, T_{CL}; as shown in Table 3, the smaller S_{a2}/S_{a1} is, the higher the charge localization temperature is. The lattice constant a along the stacking axis changes systematically together with the strength

of dimerization; then as T_{CL} increases, the lattice constant a as well as S_{a2}/S_{a1} decrease. The Néel temperature, T_N, increases as S_{a2}/S_{a1} increases; in other words, the ChTM-TTP salt with a higher charge localization temperature has a lower antiferromagnetic transition temperature.

It should be mentioned that the charge degree of freedom is lost at a higher temperature than the spin degree of freedom for (ChTM-TTP)$_2X$. The magnetic phase transition occurs in the charge localized state. This phenomenon is similar to (TMTTF)$_2$Br.[1,2] (TMTTF)$_2$Br shows a gradual increase of resistivity below 100 K, and the slope of this increase becomes large below 20 K. The SDW transition temperature of this salt is about 15 K.[44] The phase sequence of (ChTM-TTP)$_2$AuBr$_2$ is similar to this. The charge localization occurs below 100 K and the antiferromagnetic phase transition occurs at 38 K. It is difficult to decide from the present data whether this transition is a normal antiferromagnetic state or an SDW state. Since (TMTTF)$_2$Br shows superconductivity under 26 kbar (T_c = 0.8 K),[45] pressure investigation of the electrical behavior of (ChTM-TTP)$_2$AuBr$_2$ under such high pressure would be interesting.

In Jérome's phase diagram for the (TMT*C*F)$_2$X salts, (TMTTF)$_2$Br corresponds to the $P \approx 12$ kbar condition of (TMTTF)$_2$PF$_6$.[1] The recent investigation suggests that this compound changes, as the temperature decreases, from the Tomonaga–Luttinger liquid (TLL) to the charge-gaped TLL, and successively to the charge-localized antiferromagnetic ordered state.[1] For (ChTM-TTP)$_2X$, the electronic state shows a crossover from metallic to insulating region as the temperature decreases; the ground state is the antiferromagnetic insulator. This means that (ChTM-TTP)$_2X$ is located near (TMTTF)$_2$Br from the viewpoint of the phase sequence. Jérome's phase diagram shows that T_{CL} decreases as the pressure increases, and the Néel temperature increases as the pressure increases in the commensurate SDW region. Actually, these phenomena have been observed on both (TMTTF)$_2$Br and (TMTTF)$_2$PF$_6$.[44–46] The dimensionality correlates closely with the applied pressure; the pressure weakens the one-dimensionality. Although the dimerization is not explicitly related to the applied pressure, as the degree of dimerization increases, the upper half energy band separated by the dimerization gap is more perfectly isolated from the lower band. Since the upper band is half-filled (in these conductors whose overall bands are 3/4-filled), the dimerization gap enhances the effective half-filled character. As a result, the dimerization induces the charge localization. Furthermore, the pressure reduces the dimerization, because an increase of the ratio of the side-by-side to the stacking interactions ($t_\perp/t_{//}$) diminishes the dimerization gap. Pressure reduces both one-dimensionality and dimerization at the same time. The physical properties of (ChTM-TTP)$_2X$ scaled by the dimerization (S_{a2}/S_{a1}) remind us Jérome's phase diagram whose horizontal axis is changed from the pressure to the dimerization. It is characteristic of the (ChTM-TTP)$_2X$ salts that these salts show higher phase transition temperatures than those of the (TMT*C*F)$_2X$ salts in spite of the reduced on-site Coulomb repulsion U. This may be associated with the strongly dimerized structures.

Conclusion

(ChTM-TTP)$_2$AuBr$_2$, (ChTM-TTP)$_2$GaCl$_4$, and (ChTM-TTP)ReO$_4$ have been obtained by the electrocrystallization. Although the $AuBr_2^-$ and the $GaCl_4^-$ salts have 2:1 composition, the ReO_4^- salt has 1:1 composition. The $GaCl_4^-$ salt has the disordered anion structure. In both $GaCl_4^-$ and ReO_4^- salts, the dimerization of the donor molecules is much larger than that of the $AuBr_2^-$ salt. The electrical resistivity and the thermoelectric power show metallic behavior above 100 K for the $AuBr_2^-$ salt and above 150 K for the $GaCl_4^-$ salt. (ChTM-TTP)ReO$_4$ is a semiconductor owing to the dimerized 1:1 composition. The ESR spin susceptibility indicates the existence of the phase transition in the charge localized state for both $AuBr_2^-$ and $GaCl_4^-$ salts. The divergent linewidth broadening of the $GaCl_4^-$ salt indicates an antiferromagnetic phase transition. No superstructure was observed for the $AuBr_2^-$ salts down to low temperatures, and the static magnetic susceptibility of the $AuBr_2^-$ salt shows anisotropic behavior. The phase transition of (ChTM-TTP)$_2$AuBr$_2$ is not considered to be a spin-Peierls transition either; the antiferromagnetic transition is at $T_N \approx 38$ K. The ground state of both (ChTM-TTP)$_2$AuBr$_2$ and (ChTM-TTP)$_2$GaCl$_4$ is an antiferromagnetic insulator. In (ChTM-TTP)$_2X$, the magnitude of the dimerization S_{a2}/S_{a1} is a good parameter for discussing the charge localization temperature and the Néel temperature.

T. Kawamoto is grateful to the JSPS Research Fellowships for Young Scientists for financial support. This work was partly supported by a Grant in Aid for Scientific Research (No. 10440204) from the Ministry of Education, Science, Sports and Culture.

References

1 D. Jérome, *Science*, **252**, 1509 (1991); D. Jérome, P. Auban-Senzier, L. Balicas, K. Behnia, W. Kang, P. Wzietek, C. Berthier, P. Caretta, M. Horvatic, P. Segransan, L. Hubert, and C. Bourbonnais, *Synth. Met.*, **70**, 719 (1995); C. Bourbonnais, *Synth. Met.*, **84**, 19 (1997); C. Bourbonnais and D. Jérome, *Science*, **281**, 1155 (1998).

2 T. Ishiguro, K. Yamaji, and G. Saito, "Organic Superconductors," 2nd ed, Springer-Verlag, Berlin (1998).

3 V. Vescoli, L. Degiorgi, W. Henderson, G. Grüner, K. P. Starkey, and L. K. Montgomery, *Science*, **281**, 1181 (1998); A. Schwartz, M. Dressel, G. Grüner, V. Vescoli, L. Degiorgi, and T. Giamarchi, *Phys. Rev. B*, **58**, 1261 (1998).

4 J. M. Williams, J. R. Ferraro, R. J. Thorn, K. D. Carlson, U. Geiser, H. H. Wang, A. M. Kini, and M.-H. Whangbo, "Organic Superconductors (Including Fullerenes): Synthesis, Structure, Properties, and Theory," Prentice Hall, NJ (1992).

5 T. Mori, *Bull. Chem. Soc. Jpn.*, **71**, 2509 (1998); T. Mori, H. Mori, and S. Tanaka, *Bull. Chem. Soc. Jpn.*, **72**, 179 (1999); T. Mori, *Bull. Chem. Soc. Jpn.*, **72**, 2011 (1999).

6 T. Mori, T. Kawamoto, Y. Misaki, K. Kawakami, H. Fujiwara, T. Yamabe, H. Mori, and S. Tanaka, *Mol. Cryst. Liq. Cryst.*, **284**, 271 (1996).

7 Y. Misaki, N. Higuchi, H. Fujiwara, T. Yamabe, T. Mori, H. Mori, and S. Tanaka, *Angew. Chem., Int. Ed. Engl.*, **34**, 1222 (1995); Y. Misaki, N. Higuchi, T. Ohta, H. Fujiwara, T. Yamabe, T. Mori, H. Mori, and S. Tanaka, *Mol. Cryst. Liq. Cryst.*, **284**, 27 (1996).

8 M. Ashizawa, M. Aragaki, T. Mori, Y. Misaki, and T.

Yamabe, *Chem. Lett.*, **1997**, 649. The unit cell of (ChTM-TTP)$_2$Au(CN)$_2$ is chosen as $\alpha < 90°$ in this report. We can transform the unit cell from the original one to the same setting as (ChTM-TTP)$_2$AuBr$_2$. The transformed cell parameters are a = 9.764(10) Å, b = 17.18(1) Å, c = 8.87(1) Å, α = 98.47(8)°, β = 116.83(9)°, γ = 73.33(6)°, V = 1271(5) Å^3. The formula weight is not 1851.4 but 1483.2, and the calculated density is not 2.419 g cm^{-3} but 1.938 g cm^{-3}.

9 M. Ashizawa, M. Aragaki, T. Mori, Y. Misaki, and K. Tanaka, *Synth. Met.*, **102**, 1603 (1999).

10 M. Ashizawa, Master's thesis submitted to Tokyo Institute of Technology (1998), unpublished.

11 J. Schmalian, *Phys. Rev. Lett.*, **81**, 4232 (1998); H. Kondo and T. Moriya, *J. Phys. Soc. Jpn.*, **67**, 3695 (1998); H. Kino and H. Kontani, *J. Phys. Soc. Jpn.*, **68**, 1481 (1999).

12 M. C. Burla, M. Camalli, G. Cascarano, C. Giacovazzo, G. Polidori, R. Spagna, and D. Viterbo, *J. Appl. Cryst.*, **22**, 303 (1989).

13 G. M. Sheldrick, "Crystallographic Computing 3," Oxford University Press, Oxford (1985), pp. 175–189.

14 D. T. Cromer and J. T. Waber, "International Tables for X-ray Crystallography, Vol. IV," The Kynoch Press, Birmingham, England (1974), Table 2.2 A.

15 T. Mori, A. Kobayashi, Y. Sasaki, H. Kobayashi, G. Saito, and H. Inokuchi, *Bull. Chem. Soc. Jpn.*, **57**, 627 (1984). Sulfur 3d orbitals are not included in the present calculation, which reduce the total bandwidth by about 30%, and reduce the inter/intra ratio by 50% in comparison with the case including sulfur 3d orbitals in BEDT-TTF.

16 M. A. Beno, M. A. Firestone, P. C. W. Leung, L. M. Sowa, H. H. Wang, J. M. Williams, and M.-H. Whangbo, *Solid State Commun.*, **57**, 735 (1986).

17 The slip distance is defined by the slip of center of the TTP unit (C7=C8). Because ChTM-TTP is an asymmetric molecule, this is different from the overlap of the full molecular length.

18 T. Mori, H. Inokuchi, Y. Misaki, T. Yamabe, H. Mori, and S. Tanaka, *Bull. Chem. Soc. Jpn.*, **67**, 661 (1994).

19 K. Bechgaard, K. Carneiro, F. B. Rasmussen, M. Olsen, G. Rindolf, C. S. Jacobsen, H. J. Pedersen, and J. C. Scott, *J. Am. Chem. Soc.*, **103**, 2440 (1981).

20 T. Mori, T. Kawamoto, J. Yamaura, T. Enoki, Y. Misaki, T. Yamabe, H. Mori, and S. Tanaka, *Phys. Rev. Lett.*, **79**, 1702 (1997).

21 T. Mori, Y. Misaki, and T. Yamabe, *Bull. Chem. Soc. Jpn.*, **70**, 1809 (1997).

22 T. Mori, T. Kawamoto, Y. Misaki, and K. Tanaka, *Bull. Chem. Soc. Jpn.*, **71**, 1321 (1998).

23 T. Kawamoto, M. Ashizawa, M. Aragaki, T. Mori, T. Yamamoto, H. Tajima, H. Kitagawa, T. Mitani, Y. Misaki, and K. Tanaka, *Phys. Rev. B*, **60**, 4635 (1999).

24 T. Kawamoto, M. Aragaki, T. Mori, Y. Misaki, and K. Tanaka, *J. Mater. Chem.*, **8**, 285 (1998).

25 P. M. Chaikin, R. L. Greene, S. Etemad, and E. Engler, *Phys. Rev. B*, **13**, 1627 (1976).

26 K. Bechgaard, C. S. Jacobsen, K. Mortensen, H. J. Pedersen, and N. Thorup, *Solid State Commun.*, **33**, 1119 (1980).

27 K. Saito, M. Ishibashi, H. Yoshino, T. Mochiduki, H. Saitoh, H. Itoh, K. Kikuchi, and I. Ikemoto, *Synth. Met.*, **52**, 87 (1992).

28 The resistivity of (ChTM-TTP)ReO$_4$ was measured by the two-probe method because of the short length of the crystals.

29 T. Sugano, G. Saito, and M. Kinoshita, *Phys. Rev. B*, **34**, 117 (1986); **35**, 6554 (1987).

30 S. Flandrois, C. Coulon, P. Delhaes, D. Chasseau, C. Hauw, J. Gaultier, J. M. Fabre, and L. Giral, *Mol. Cryst. Liq. Cryst.*, **79**, 307 (1982).

31 P. Delhaes, C. Coulon, J. Amiell, S. Flandrois, E. Toreilles, J. M. Fabre, and L. Giral, *Mol. Cryst. Liq. Cryst.*, **50**, 43 (1979).

32 H. J. Pedersen, J. C. Scott, and K. Bechgaard, *Solid State Commun.*, **35**, 207 (1980); *Phys. Rev. B*, **24**, 5014 (1981).

33 M. Dumm, A. Loidl, B. Fravel, K. P. Starkey, L. K. Montgomery, and M. Dressel, *Phys. Rev. B*, **61**, 511 (2000).

34 K. Mortensen, Y. Tomkiewicz, and K. Bechgaard, *Phys. Rev. B*, **25**, 3319 (1982).

35 S. S. P. Parkin, J. C. Scott, J. B. Torrance, and E. M. Engler, *Phys. Rev. B*, **26**, 6319 (1982); *J. Phys. (Paris), Colloq.*, **44**, C3-1111 (1983).

36 K. Enomoto, Master's thesis submitted to Tokyo Institute of Technology (2000), unpublished.

37 Y. Misaki, H. Nishikawa, K. Kawakami, S. Koyanagi, T. Yamabe, and M. Shiro, *Chem. Lett.*, **1992**, 2321.

38 T. Mori, T. Kawamoto, K. Iida, J. Yamaura, T. Enoki, Y. Misaki, T. Yamabe, H. Mori, and S. Tanaka, *Synth. Met.*, **103**, 1885 (1999).

39 T. Mori, Y. Misaki, T. Yamabe, H. Mori, and S. Tanaka, *Chem. Lett.*, **1995**, 549.

40 Y. Misaki, T. Miura, M. Taniguchi, H. Fujiwara, T. Yamabe, T. Mori, H. Mori, and S. Tanaka, *Adv. Mater.*, **9**, 714 (1997).

41 (ChTM-TTP)$_2X$ is classified as the β_{21}-type according to Mori's notation.

42 P. M. Grant, *J. Phys. (Paris), Colloq.*, **44**, C3-847 (1983).

43 L. Ducasse, M. Abderrabba, J. Hoarau, M. Pesquer, B. Gallois, and J. Gaultier, *J. Phys. C*, **19**, 3805 (1986).

44 T. Takahashi, F. Creuzet, D. Jérome, and J. M. Fabre, *J. Phys. (Paris), Colloq.*, **44**, C3-1095 (1983).

45 L. Balicas, K. Behnia, W. Kang, E. Canadell, P. Auban-Senzier, D. Jérome, M. Ribault, and J. M. Fabre, *J. Phys. I (France)*, **4**, 1539 (1994).

46 D. S. Chow, P. Wzietek, D. Fogliatti, B. Alavi, D. J. Tantillo, C. A. Merlic, and S. E. Brown, *Phys. Rev. Lett.*, **81**, 3984 (1998).